ACS OMEGA

Article

Cite This: ACS Omega 2019, 4, 10834−10844

http://pubs.acs.org/journal/acsodf

Removal of Heavy Metal Water Pollutants (Co^{2+} and Ni^{2+}) Using Polyacrylamide/Sodium Montmorillonite (PAM/Na-MMT) Nanocomposites

Kariana Moreno-Sader,*[,†,§] Alvaro García-Padilla,[†,§] Alvaro Realpe,[†] María Acevedo-Morantes,[†] and João B. P. Soares[‡]

[†]Department of Chemical Engineering, University of Cartagena, Avenida Consulado St. 30 #48-152, 130015 Cartagena de Indias, Colombia

[‡]Department of Chemical and Materials Engineering, University of Alberta, 116 St. and 85 Ave., T6G 2R3 Edmonton, Canada

ABSTRACT: Nanocomposites composed of polyacrylamide and nanoclay were synthesized via free-radical cross-linking polymerization and used to adsorb Co^{2+} and Ni^{2+} ions from water. The polyacrylamide (PAM)/sodium montmorillonite (Na-MMT) nanocomposites were characterized by Fourier transform infrared spectroscopy, X-ray diffraction, and scanning electron microscopy to confirm the interaction between montmorillonite and the polymer matrix. The effects of pH and heavy metal ion concentration on the adsorption capacity of PAM/Na-MMT were evaluated to determine suitable operating conditions for further experiments. Batch adsorption experimental data were fitted to Langmuir and Freundlich models, which provided information about the adsorption mechanism and the adsorbent surface. The highest Ni^{2+} removal yield was found to be 99.3% using the 2:1 (w/w) nanocomposite at pH 6 in 100 ppm of Ni^{2+} solution. The Co^{2+} removal yield was 98.7% at pH 6 in 60 ppm of Co^{2+} solution using the 4:1 (w/w) nanocomposite. These results were higher than those obtained by polyacrylamide and nanoclay under the same conditions (removal yield between 87.40 and 94.50%), indicating that PAM/Na-MMT nanocomposites remove heavy metal water pollutants more efficiently and can be used as a novel adsorbent for further industrial applications.

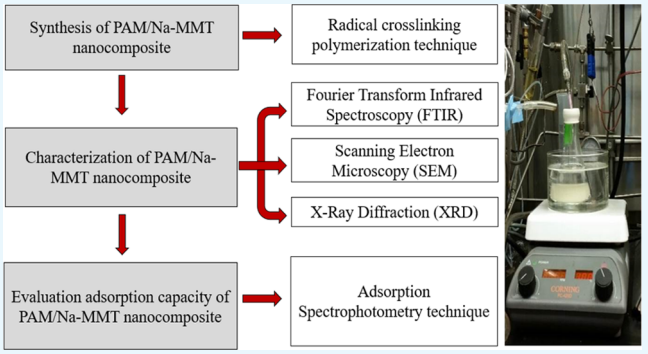

1. INTRODUCTION

Water pollution is a major global environmental problem due to its effect on living organisms and on the equilibrium of the whole ecosystem. A wide range of toxic derivatives, including heavy metals, suspended particles, aromatic compounds, and chemicals dyes are discharged in water sources.[1] Contamination with heavy metals caused by metal plating facilities, mining operations, fertilizer industries, tanneries, batteries, paper industries, and pesticides, among others has become the focus of attention of researchers and policy makers due to the high level of these pollutants in the environment.[2] Currently, ten heavy metals are of major public health concern: led, arsenic, cadmium, chromium, cobalt, copper, mercury, manganese, zinc, and nickel.[3] Their high solubility in water makes them easily absorbed by aquatic living organisms, causing them to accumulate in the environment and reach hazardous concentration levels.[4,5] In this paper, we will focus our attention on cobalt and nickel; exposure to cobalt compounds may cause adverse effects such as vomiting, heart failure, and nausea,[6,7] whereas exposure to nickel may produce human health problems such as contact dermatitis.[8]

Recently, numerous approaches have been developed to remove heavy metals from water (such as chemical precipitation, ion exchange, and reverse osmosis), but some of these are considered too expensive and inadequate to treat water pollutants.[9] Adsorption has been considered an attractive alternative to decrease the amount of heavy metals in wastewater due to the availability of low cost, ecofriendly, high-efficiency adsorbents.[4,10] Novel adsorbents have been also developed to improve the selectivity, adsorption capacity, and reusability for large-scale application of traditional adsorbents.[7] Compared to other conventional adsorbents such as starch,[11] activated carbon,[6] chitosan,[12] and graphene oxides,[13] high-molecular-weight acrylamide-based polymers are promising adsorbents for heavy metal removal due to their ability to increase adsorption performance at a relatively low cost.[14,15]

Recent research on this area has focused on polyacrylamide and its modification with starch, chitosan, guar gum, and nanoclay to improve its properties as an adsorbent (such as Brunauer−Emmett−Teller surface area, total pore volume, and pore diameter).[1,16−18] Hayati et al.[19] studied the adsorption capacity of nanocomposites based on carbon nanotubes (CNs)

Received: April 5, 2019
Accepted: June 10, 2019
Published: June 21, 2019

DOI: 10.1021/acsomega.9b00981
ACS Omega 2019, 4, 10834−10844

and PAM for the removal of Ni^{2+}, Zn^{2+}, As^{3+}, and Co^{2+}. They characterized these new materials by Fourier transform infrared (FTIR), scanning electron microscopy (SEM), and transmission electron microscopy (TEM) and evaluated their adsorption performances for different initial metal ion concentrations, temperatures, solution pH values, nanocomposite dosages, and contact times. The results indicated that Ni^{2+} was more easily adsorbed by PAM/CN than the others heavy metals and that a pH of 8 is the most suitable condition for maximum adsorption. On the other hand, Zhao et al.[20] synthesized a superadsorbent based on polyacrylamide and bentonite for the adsorption of Cu^{2+}. They also evaluated the effect of pH, heavy metals initial concentration, and ionic strength on the adsorption percentage. The highest adsorption capacity of 97%, which was achieved at a pH of 7 in 10 mg/L of Cu^{2+} solution, suggested that this nanocomposite could be used successfully to remove Cu^{2+} from aqueous solutions.

In this work, a surfactant-free dispersion radical cross-linking polymerization was carried out to synthesize acrylamide and sodium montmorillonite (Na-MMT) nanocomposites. The nanoclay/polymer-based matrix nanocomposites were evaluated at three different ratios of acrylamide (AAm) to Na-MMT (1:1, 2:1, and 4:1 w/w). These nanomaterials were characterized by FTIR, X-ray diffraction (XRD), and SEM to observe the chemical structure, the degree of intercalation, and the morphology, respectively. The Co^{2+} and Ni^{2+} removal yield from aqueous solution was evaluated at different pH values (3, 4.5, and 6) and heavy metal initial concentrations (20, 60, 100, 140, and 180 ppm). The residual concentration of heavy metals after a contact time of 24 h was measured by atomic absorption spectroscopy, and these results were used to construct Langmuir and Freundlich isotherms.

2. MATERIALS AND METHODS

2.1. Experimental Materials. Acrylamide (AAm, ≥98%, MW = 71.08 g/mol), ammonium persulfate (APS, ≥98%), *N*,*N*′-methylene-(bis)-acrylamide (MBA, 99%), *N*,*N*,*N*′,*N*′-tetramethyl-ethylenediamine (TEMED, 99%), poly-(vinylpyrrolidone) (PVP, average mol wt 40 000), nickel(II) chloride hexahydrate (99.9% trace metals basis), and cobalt(II) chloride hexahydrate (reagent grade) were purchased from Sigma Aldrich. Sodium montmorillonite nanoclay (commercially referred as Cloisite Na^+) was obtained from Southern Clays. Deionized water and ethanol of analytical grades were used as solvents during cross-linking polymerizations.

2.2. Synthesis of Nanocomposites. The polyacrylamide/Na-MMT nanocomposites were synthesized using different clay-to-monomer ratios to evaluate the effect of Na-MMT amount on the adsorbent capacity for Co^{2+} and Ni^{2+} uptake. It is important to point out that AAm loading affects the intercalation degree of Na-MMT, affecting the adsorption capacity of these materials.[21] The purpose of nanocomposite preparation lies on increasing the interlayer space of nanoclay that makes possible a greater exchange of metallic ions. PAM was selected as the polymer matrix due to its ability to interact with the clay surface via its amide groups.[22] In addition, these amide functional groups (as well as alcohol and amine groups) are important for the removal of Ni^{2+} and Co^{2+} due to their strong interaction with substrates. Since monomer cross-linking is widely used to disperse clay sheets in polymer composites,[10] it was selected as technique to prepare these nanocomposites. All reactions were conducted below 50 °C due to low temperature polymerizations promote the synthesis of high-molecular-weight PAM.[23] To assure an efficient dispersion of the clay particles in PAM, vigorous stirring was kept throughout the polymerization.[24] Since oxygen scavenges off free radicals during AAm polymerization, the polymerizations were carried out under an inert nitrogen atmosphere.[25]

Such nanocomposites were prepared according to the procedure described by Atta et al.[10] A solution of 100 mL of water/ethanol (60/40 vol %) was used to disperse different amounts of Na-MMT, which are summarized in Table 1.

Table 1. Experimental Conditions for Polymerization Runs to Synthetize the Nanocomposite

nanocomposite type	Na-MMT (g)	AAm (g)	PVP (g)
PAM/Na-MMT nanocomposite (1:1)	2	2	0.3
PAM/Na-MMT nanocomposite (2:1)	1	2	0.15
PAM/Na-MMT nanocomposite (4:1)	0.5	2	0.075

Afterward, PVP was added as a stabilizer under vigorous stirring for 24 h. The surfactant-free dispersion radical cross-linking polymerization was carried out under an inert nitrogen atmosphere at 40 °C. The monomer was dispersed in 50 mL of the previously prepared Na-MMT suspension. A solution of APS at 0.01 g/mL was used as a radical initiator to start the polymerization. The reaction temperature was gradually increased to 50 °C, and the remaining Na-MMT suspension was added dropwise during 1 h. Subsequently, the remaining amounts of AAm, MBA, and TEMED were dispersed into the other 50 mL of Na-MMT suspension and this mixture was injected dropwise during 1 h. Then, dilution of APS was introduced into the reactor and the reaction temperature was decreased to 45 °C. After 24 h of continuous stirring, the reaction mixture was repeatedly centrifuged at 10 000 rpm and rinsed with ethanol to remove impurities and the PAM homopolymer. Finally, the product was dried under vacuum at 30 °C, pulverized by a mortar pestle, and sieved through a 100 mesh screen.[24]

2.3. Characterization Techniques. *2.3.1. FTIR Analysis.* FTIR spectra of commercial nonionic polyacrylamide, Cloisite Na^+, and nanocomposite (1:1, 2:1, and 4:1 w/w) samples were recorded on a Cary FTIR Model 660 (Agilent Technologies) by acquiring 64 scans with 4 cm^{-1} resolution in the 4000−400 cm^{-1} region on attenuated total reflection (ATR) mode.

2.3.2. XRD Analysis. The XRD patterns of PAM/Na-MMT nanocomposites and its base materials (PAM and Cloisite Na^+) were recorded using a Rigaku Ultima IV diffractometer with Co Kα (λ = 0.1789 nm) radiation. The diffraction intensities were recorded from 5 to 40° (2θ) angle. The *d*-spacing of MMT layers was calculated using the Bragg equation

$$2d \sin(\theta) = n\lambda \quad (1)$$

where θ is the diffraction angle, *n* is the order of diffraction, and λ is the incident wavelength.

2.3.3. SEM Analysis. SEM analyses of nanocomposite samples were carried out on a Sigma HD Zeuss scanning electron microscope at an acceleration voltage of 20 kV (SE detector). The main objective of this characterization technique is the identification of materials morphology that represents a key factor to analyze in the adsorption process.

2.4. Adsorption Experiments. The adsorption of Co^{2+} and Ni^{2+} onto PAM/Na-MMT was analyzed by varying the initial concentrations (20, 60, 100, 140 and 180 ppm) of these heavy

DOI: 10.1021/acsomega.9b00981
ACS Omega 2019, 4, 10834−10844

metal ions. All batch experiments were carried out under ambient conditions (20 °C). In this respect, the pH values of stock solutions (3, 4.5, and 6) were adjusted using 0.1 M HCl and NaOH in negligible volumes. Afterward, 50 mL of stock solutions and 0.1 g of nanocomposite were added to a beaker placed on a stirring plate. The contact time was fixed to 24 h. After adsorption, the separation of solid and liquid phases was performed by centrifugation at 10 000 rpm for 30 min. The supernatant (1 mL) was separated to measure its residual heavy metal concentration through atomic absorption spectrometry (VARIAN 220 FS) with air-acetylene flame technique. The pH was also measured at the end of batch experiments with nonsignificant variations with respect to its initial value. The amount of Co^{2+} and Ni^{2+} ions adsorbed onto PAM/Na-MMT at equilibrium and the removal yield were calculated with the following equations

$$q_e = (C_o - C_e) \times \frac{V}{m} \quad (2)$$

$$\text{removal yield } (\%) = \frac{(C_o - C_e)}{C_o} \times 100\% \quad (3)$$

where C_o and C_e (mg/L) are the initial concentration of metal ions and equilibrium concentration in the supernatant after centrifugation, respectively, V is the volume of the solution (L), m is the mass of adsorbent (g), and q_e is the amount of heavy metals ions adsorbed per weight unit of adsorbent after equilibrium (mg/g).

After analyzing the influence of solution pH and initial concentration of both heavy metals, it was selected the optimum conditions to perform further adsorption processes using PAM/Na-MMT nanocomposites. Then, the sorption performance of these nanocomposites was compared with the adsorption removal yields that can achieve separately polyacrylamide and nanoclay under the same conditions of initial pH and concentration. This comparison is needed to judge whether it is worth incorporating polyacrylamide into the interlaminar space of MMT nanoclay.

3. RESULTS AND DISCUSSION

3.1. Characterization of Nanocomposites. *3.1.1. FTIR Spectra.* The FTIR spectra for nanoclay, polyacrylamide, and three PAM/Na-MMT nanocomposites made at different ratios of AAm to Na-MMT (1:1, 2:1, and 4:1 w/w) are compared in Figure 1.

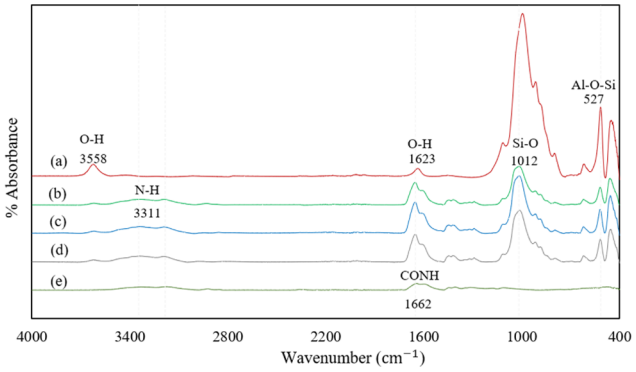

Figure 1. FTIR spectra of (a) Na-MMT nanoclay, (b) PAM/Na-MMT nanocomposite (1:1), (c) PAM/Na-MMT nanocomposite (2:1), (d) PAM/Na-MMT nanocomposite (4:1), and (e) PAM.

The FTIR spectra of the nanoclay shows H−O−H bending vibrations related to interlayer water molecules at 1623 cm^{-1}.[26,27] The characteristic adsorption band assigned to the stretching vibrations of AlOH and SiOH was observed at 3558 cm^{-1}.[2828] The Na-MMT structure consists of 2:1 layers formed by two silica tetrahedral sheets linked with an alumina octahedral sheet;[29,30] hence, the presence of this functional groups was expected. In the spectra of the nanocomposites (Figure 1b−d), this peak shifted to lower frequencies, perhaps due to interactions between the functional groups of PAM and Na-MMT.[31] The peak at 3311 cm^{-1} was attributed to the NH_2 group, which is also observed in the spectrum of commercial polyacrylamide (Figure 1e).[24] The peak at 1662 cm^{-1} was assigned to the stretching vibration of the C═O group.[10] In addition, the CH groups from the backbone of PAM were observed at 1459 cm^{-1}.[32] The presence of amide functional groups, as well as alcohol and amine groups, contributes to the formation of strong hydrogen bonds.[33] The sharpest adsorption band of montmorillonite was identified at 958 cm^{-1}, which is related to stretching vibrations of Si−O bonds in the tetrahedral layer.[34,35] In addition, peaks at 950 and 575 cm^{-1} were assigned to Al−Al−OH[34,36] and Si−O−Al,[35] respectively. The fact that PAM/Na-MMT nanocomposites exhibit characteristic adsorption bands of nanoclays indicates a successful synthesis due to the incorporation of the polymer matrix into Na-MMT nanoclay layers.[10]

3.1.2. XRD Analysis. XRD analysis was performed to study structural variations in the Na-MMT galleries due to the dispersion of PAM and to determine possible intercalation or exfoliation phenomena.[37] Figure 2 displays XRD patterns for PAM, nanocomposites (1:1, 2:1, and 4:1 w/w), and the Na-MMT nanoclay.

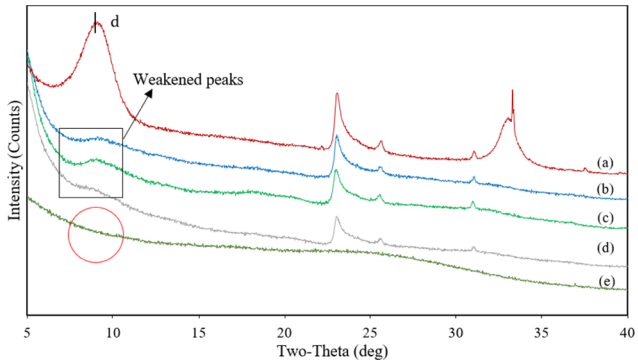

Figure 2. XRD patterns of (a) Na-MMT nanoclay, (b) PAM/Na-MMT nanocomposite (1:1), (c) PAM/Na-MMT nanocomposite (2:1), (d) PAM/Na-MMT nanocomposite (4:1), and (e) PAM.

The interlaminar distance $d(001)$ was calculated using eq 1 and the 2θ angle measured by XRD. Figure 2a shows a sharp peak for Na-MMT nanoclay at 2θ of 9.12°, which corresponds to $d(001)$ = 1.12 nm, a value similar to those reported in other studies.[31,38−44] The spectra for the nanocomposites (Figure 2b−d) also exhibited a weakened peak in the $d(001)$-position with a nonsignificant displacement, which may indicate the formation of a slightly intercalated montmorillonite structures and incomplete exfoliation. This means that the distance between clay layers increase, but they retain, at least partially, their original morphology in the nanocomposite.[45,46] The lack of complete exfoliation in the PAM/Na-MMT nanocomposite might have been caused by insufficient stirring during the

DOI: 10.1021/acsomega.9b00981
ACS Omega 2019, 4, 10834−10844

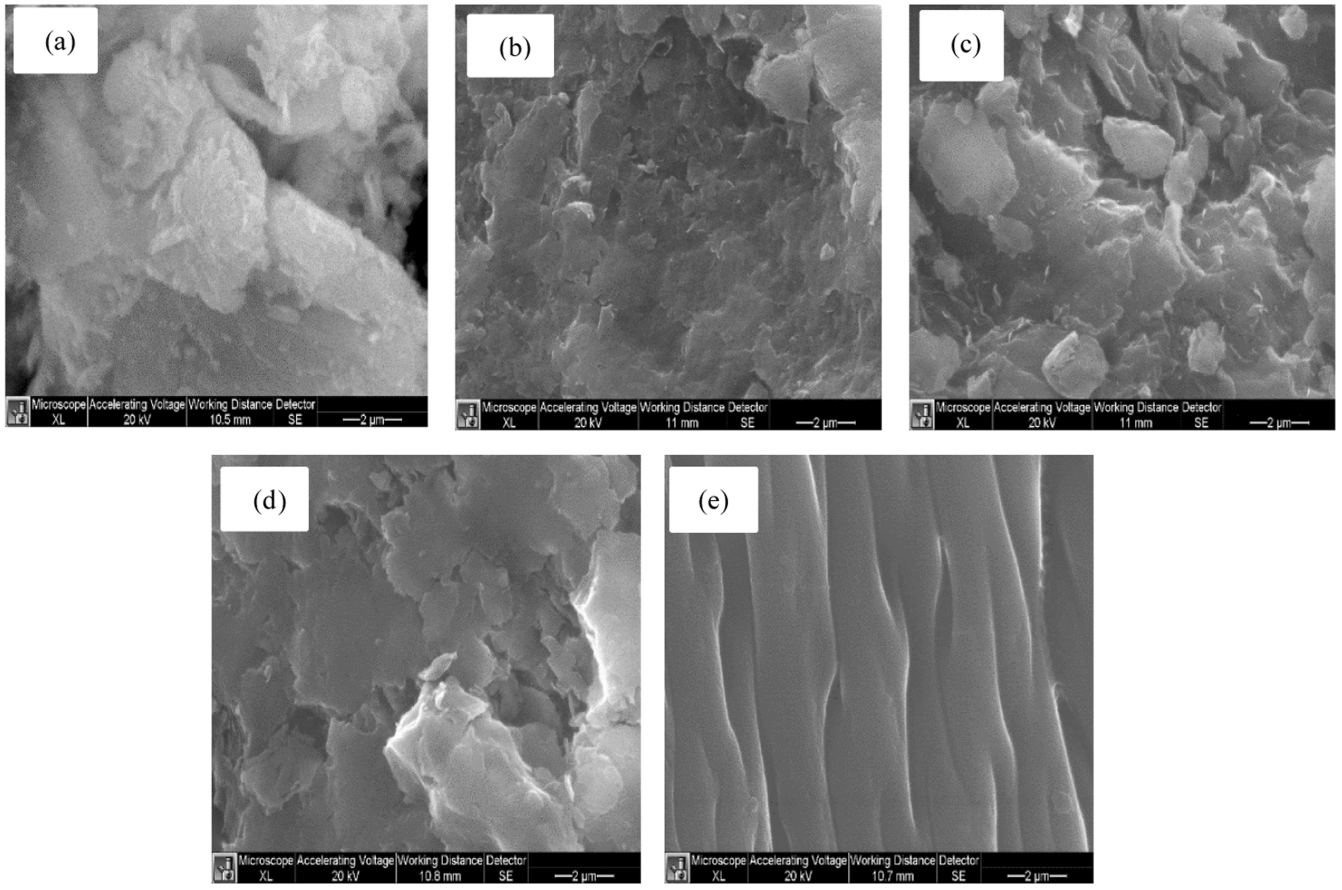

Figure 3. SEM micrographs of (a) Na-MMT nanoclay, (b) PAM/Na-MMT nanocomposites (1:1), (c) PAM/Na-MMT nanocomposites (2:1), (d) PAM/Na-MMT nanocomposites (4:1), and (e) PAM.

polymerization,[24] which were not enough to overcome the attractive electrostatic and van der Waals forces between the Na-MMT layers, as suggested by other authors.[10,45] In addition, good interfacial interactions have been reported to greatly affect the formation of intercalated and exfoliated structures, which occur when polarities of polymer surfaces and clays are similar.[47,48]

3.1.3. SEM Micrographs. The morphology of the PAM/Na-MMT nanocomposites was characterized by the SEM technique to help visualize the interaction between the clay layers and the polymer matrix.[24] Figure 3 compares SEM micrographs of PAM, nanoclay, and nanocomposites. The commercial polyacrylamide micrograph (Figure 3e) displays a regular structure with smooth surface morphology.[49] After adding Na-MMT nanoclay, the PAM morphology changed drastically, as it formed agglomerates with the nanoclay particles, indicating the dispersion of the clay layers into the polymer matrix.[24] The micrograph of Na-MMT nanoclay (Figure 3a) shows that it is composed of flakes or agglomerates of variable sizes. As the ratio of AAm to Na-MMT increases from Figure 3b to 3d, a higher number of "smoother" domains appear due to the higher ratio of PAM to nanoclay.

3.2. Adsorption Studies. *3.2.1. Adsorption Isotherms.* Adsorption is a dynamic process that is commonly described by isotherms, determined by fitting mathematical models to experimental data.[5] The information provided by these models quantifies how the adsorbate is distributed between the solid and liquid phases.[50] In this investigation, the Langmuir, eq 4, and the Freundlich, eq 5, isotherms were used to study the equilibrium adsorption of Co^{2+} and Ni^{2+} ions onto PAM/Na-MMT nanocomposites (1:1, 2:1, and 4:1 w/w). The suitability of both models was quantified with the correlation coefficient (R^2) obtained from linear fitting and adsorption capacity (q_e).[51]

$$\frac{C_e}{q_e} = \frac{1}{K_L\, q_m} + \frac{C_e}{q_m} \tag{4}$$

$$\ln q_e = \ln K_F + \left(\frac{1}{n}\right)\ln C_e \tag{5}$$

In eqs 4 and 5, q_m is the amount of heavy metal present in a monolayer (mg/g), C_e is the equilibrium concentration of heavy metal remaining in the solution (mg/L), q_e is the quantity of the heavy metal adsorbed by per unit of adsorbent at equilibrium (mg/g), K_L is the Langmuir constant (L/mg), K_F is the Freundlich constant (mg/g), and $(1/n)$ is the heterogeneity factor.[50]

The equilibrium adsorption experimental data is shown in Figure 4. The resulting isotherm parameters are summarized in Tables 2 and 3.

Comparing the correlation coefficients (R^2) obtained by fitting the adsorption results with the Langmuir and Freundlich isotherms for both Co^{2+} and Ni^{2+}, the Langmuir isotherm provided a better description of the data than the Freundlich isotherm for pH values of 4.5 and 6, but when the pH was 3, the Freundlich isotherm outperformed the Langmuir isotherm. This suggests that a monolayer adsorption process on homogeneous sites (described by the Langmuir isotherm) takes place in aqueous solutions with lower acidity. At lower pH values, the Langmuir model may deviate from the real adsorption behavior

DOI: 10.1021/acsomega.9b00981
ACS Omega 2019, 4, 10834−10844

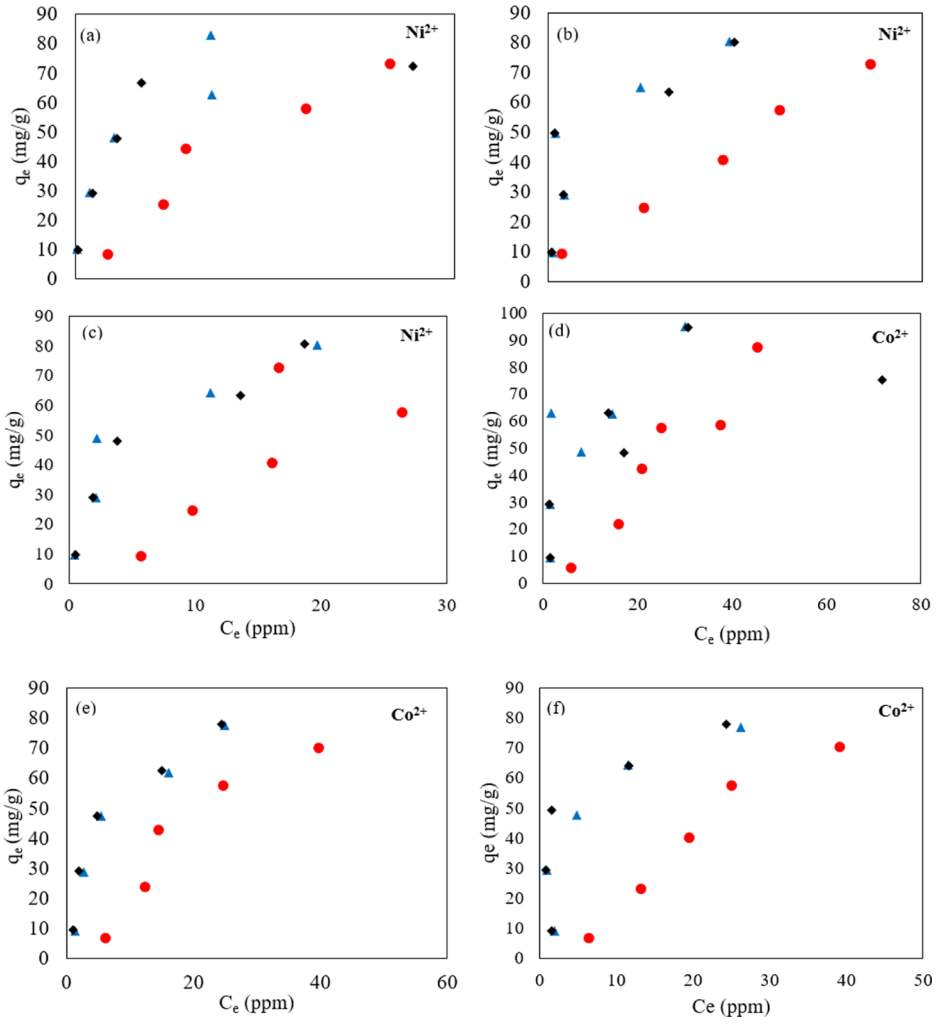

Figure 4. Heavy metal adsorption on nanocomposite at pH values of 3 (●), 4.5 (▲), 6 (♦): (a) PAM/Na-MMT nanocomposite (1:1) and Ni^{2+} ions, (b) PAM/Na-MMT nanocomposite (2:1) and Ni^{2+} ions, (c) PAM/Na-MMT nanocomposite (4:1) and Ni^{2+} ions, (d) PAM/Na-MMT nanocomposite (1:1) and Co^{2+} ions, (e) PAM/Na-MMT nanocomposite (2:1) and Co^{2+} ions, and (f) PAM/Na-MMT nanocomposite (4:1) and Co^{2+} ions.

Table 2. Isotherm Parameters for the Adsorption of Ni^{2+} Ions

			pH		
isotherm model	parameter	ratio AAm/Na-MMT	3	4.5	6
Langmuir	K_L (L/mg)	1:1	0.009	0.437	0.448
		2:1	0.036	0.34	0.47
		4:1	−0.012	0.288	0.237
	q_m (mg/g)	1:1	322.58	81.97	76.92
		2:1	119.05	90.91	83.33
		4:1	−158.73	91.74	92.59
	R^2	1:1	0.26	0.94	0.99
		2:1	0.65	0.97	0.97
		4:1	0.13	0.98	0.97
Freundlich	K_F (mg/g)	1:1	3.06	22.40	20.93
		2:1	6.93	24.83	26.67
		4:1	1.20	20.14	17.52
	n	1:1	1.06	2.17	2.29
		2:1	1.58	2.37	2.65
		4:1	0.78	1.97	1.83
	R^2	1:1	0.94	0.97	0.89
		2:1	0.89	0.86	0.84
		4:1	0.85	0.89	0.94

DOI: 10.1021/acsomega.9b00981
ACS Omega 2019, 4, 10834−10844

Table 3. Isotherm Parameters for the Adsorption of Co^{2+} Ions

isotherm model	parameter	ratio AAm/Na-MMT	pH 3	pH 4.5	pH 6
Langmuir	K_L (L/mg)	1:1	−0.011	0.118	0.158
		2:1	−0.007	0.142	0.097
		4:1	−0.012	0.107	0.163
	q_m (mg/g)	1:1	−107.53	114.94	84.75
		2:1	−222.22	98.04	108.69
		4:1	−103.09	106.38	97.09
	R^2	1:1	0.40	0.81	0.95
		2:1	0.09	0.95	0.90
		4:1	0.36	0.70	0.77
Freundlich	K_F (mg/g)	1:1	0.63	20.98	15.53
		2:1	1.06	11.15	13.91
		4:1	0.66	17.46	22.54
	n	1:1	0.76	2.31	2.28
		2:1	0.82	1.54	1.72
		4:1	0.75	2.14	2.61
	R^2	1:1	0.96	0.49	0.72
		2:1	0.89	0.86	0.84
		4:1	0.96	0.54	0.43

due to the assumption of no interactions between sorbate molecules. Nevertheless, this model provides satisfactory interpretations of a wide number of experiments that mainly present chemisorption.[5] On the other hand, the Freundlich isotherm models multilayer adsorption processes on heterogeneous surfaces and its better fit suggests that this mechanism describes the process at pH 3 more accurately.

As is widely known, the concept of linearity is not enough in accepting or rejecting a model; therefore, information about the main adsorption mechanism given by model parameters needs to be analyzed.[50,52] The Langmuir constant parameter was used to determine the dimensionless separation factor R_L, which confirms the favorability of the adsorption process[53]

$$R_L = \frac{1}{1 + K_L C_o} \quad (6)$$

Because the Langmuir isotherm did not fit the data collected at pH 3, R_L was only calculated for pH values of 4.5 and 6. The values obtained for the dimensionless separation factor are shown in Figure 5.

The PAM/Na-MMT nanocomposites (1:1) showed values of $0.012 < R_L < 0.1$ for Ni^{2+} ions and $0.028 < R_L < 0.297$ for Co^{2+} ions. For the PAM/Na-MMT nanocomposites (2:1), $0.012 < R_L < 0.129$ for and $0.038 < R_L < 0.34$ for Ni^{2+} and Co^{2+} ions, respectively. The dimensionless separation factor may take the value $R_L = 0$ for irreversible, between $0 < R_L < 1$ for favorable, $R_L = 1$ for linear, or $R_L > 1$ for unfavorable adsorption processes.[52] Figure 5 shows that all values obtained for R_L are between 0 and 1, so the adsorption process on PAM/Na-MMT nanocomposites can be identified as favorable, tending to irreversibility at low initial concentrations of heavy metal ions. Because irreversible adsorption occurs slowly, the desorption of the adsorbed species may be undetectable during the time interval of the experiments.[54] This work did not study desorption; thus, it is not possible to determine if irreversible adsorption took place for R_L very close to zero.

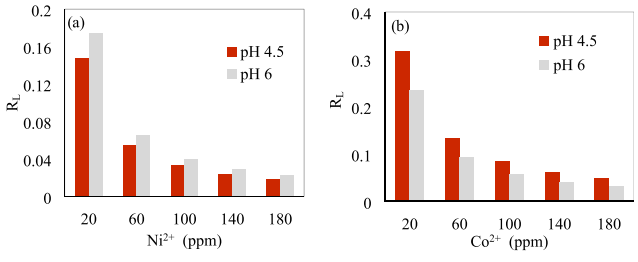

Figure 5. R_L dimensionless factor versus initial concentration for (a) Ni^{2+} ions and (b) Co^{2+} ions at pH values of 4.5 and 6 with the PAM/Na-MMT nanocomposite (4:1).

Figure 6 displays the heterogeneity factor $1/n$ of the Freundlich isotherm for PAM/Na-MMT nanocomposites,

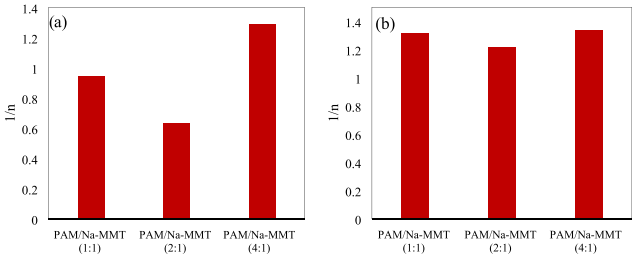

Figure 6. Heterogeneity factor of the Freundlich adsorption model for (a) Ni^{2+} ions and (b) Co^{2+} ions at pH 3.

which provides information on the adsorption mechanism and surface heterogeneity. Cooperative (multilayer) adsorption occur when $1/n > 1$, and mainly chemisorption takes place when $1/n < 1$.[5] Most values for the heterogeneity factor of Ni^{2+} are less than 1, suggesting that the adsorption process onto the nanocomposites with greater concentration of montmorillonite is mostly affected by chemisorption. The PAM/Na-MMT (4:1) nanocomposite reported the heterogeneity factor greater than 1, similar to those results when Co^{2+} ions are removed, suggesting a cooperative adsorption in all of these scenarios. A heterogeneous surface is represented for $1/n$ approaching to zero; thus, adsorption of heavy metal ions may occur at homogeneously distributed active sites of PAM/Na-MMT nanocomposites instead of heterogeneous one; on the basis of that, $1/n$ is not close to zero for any of the synthetized nanocomposites.

DOI: 10.1021/acsomega.9b00981
ACS Omega 2019, 4, 10834−10844

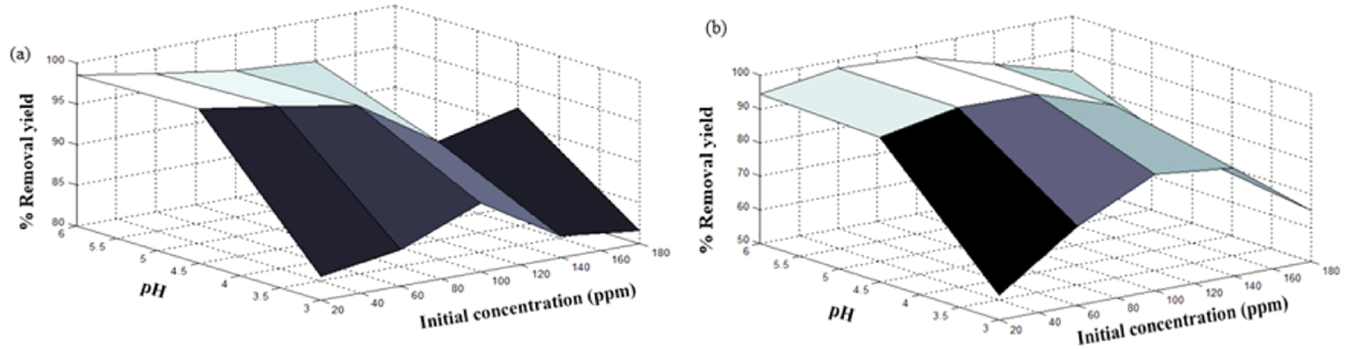

Figure 7. Effects of initial concentration and pH on removal yield (%) of (a) Ni^{2+} ions and (b) Co^{2+} ions using the PAM/Na-MMT nanocomposite (1:1).

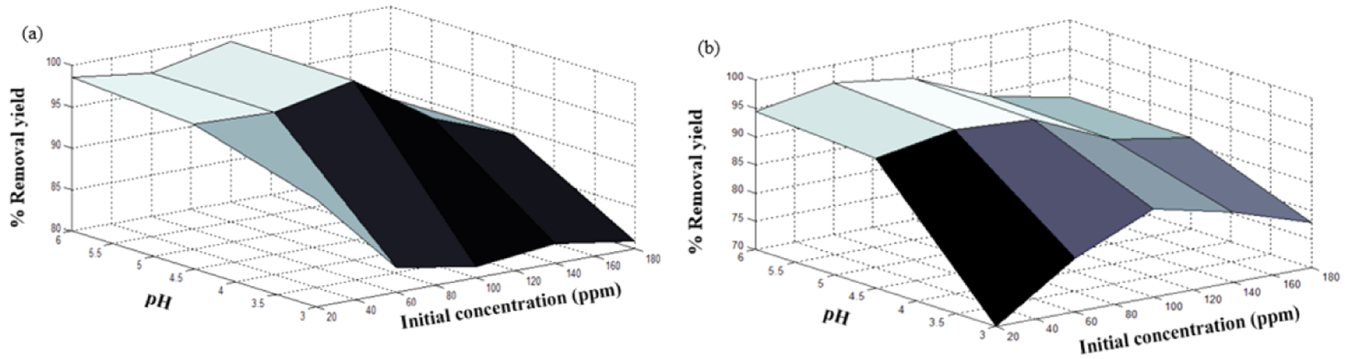

Figure 8. Effects of initial concentration and pH on removal yield (%) of (a) Ni^{2+} ions and (b) Co^{2+} ions using the PAM/Na-MMT nanocomposite (2:1).

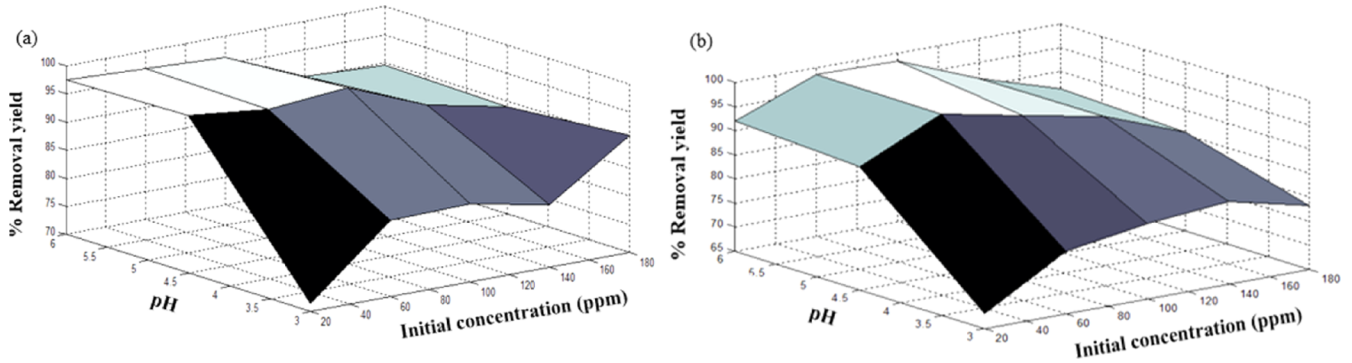

Figure 9. Effects of initial concentration and pH on removal yield (%) of (a) Ni^{2+} ions and (b) Co^{2+} ions using the PAM/Na-MMT nanocomposite (4:1).

3.2.2. Influence of pH and Initial Concentration on Removal Yield of Heavy Metals. Figures 7–9 show the effect of both operational parameter on the removal yield of heavy metal ions using nanocomposites (1:1, 2:1, and 4:1 w/w). One of the most influential parameters during the adsorption process is the pH, which affects the adsorption mechanism and the uptake capacity. As shown in these surface plots, the lowest removal yields were achieved at pH 3, which may be attributed to the competition between attractive and repulsive interactions caused by modifying the polyacrylamide structure and its properties when protonation of amine and hydroxyl groups takes place.[33] Therefore, a high H_3O^+ concentration at low pH decreased the number of binding sites for Ni^{2+} and Co^{2+} ions and, therefore, decreased the adsorption capacity of the nanocomposite.[50]

The initial concentration of Ni^{2+} and Co^{2+} solution also plays an important role in the adsorption process because it provides the driving force required to surmount all of the mass transfer limitations of heavy metal ions between the aqueous and solid phases.[55] It was observed that a high initial concentration of heavy metal ions reduced the removal yield, which may be attributed to the saturation of available sites onto the adsorbent surface. Hence, an initial concentration from 60 to 100 ppm was considered optimum for these experimental conditions. It was found that the highest Co^{2+} removal yield of 98.67% was reached at pH 6 and C_o of 60 ppm using the PAM/Na-MMT nanocomposite (4:1 w/w). For the Ni^{2+} uptake process, the highest removal yield of 99.3% was obtained at pH 6 and C_o of 100 ppm using the PAM/Na-MMT nanocomposite (2:1 w/w). These optimum results of adsorption yields were compared to those obtained using PAM and Na-MMT under the same

DOI: 10.1021/acsomega.9b00981
ACS Omega 2019, 4, 10834−10844

conditions of pH and concentration. Table 4 lists the removal yields achieved by PAM, Na-MMT, and the nanocomposite for nickel and cobalt sorption. This comparison revealed that the PAM/Na-MMT nanocomposite features higher sorption capacity than that of its base compounds, i.e., polyacrylamide and nanoclay, which may be attributed to the increase in ion exchange capacity after increasing the interlayer space of Na-MMT.

Table 4. Comparison of Co^{2+} and Ni^{2+} Adsorption Capacity of PAM, Na-MMT, and the PAM/Na-MMT Nanocomposite

adsorbent	Co^{2+} removal yield (%)[a]	Ni^{2+} removal yield (%)[b]
polyacrylamide (PAM)	87.40	90.20
sodium montmorillonite (Na-MMT)	89.17	94.50
PAM/Na-MMT nanocomposite	98.67	99.30

[a]pH = 6 and C_o = 60 ppm. [b]pH = 6 and C_o = 100 ppm.

4. CONCLUSIONS

This research project evaluated the adsorption capacity of nanocomposites based on PAM and montmorillonite for the removal of heavy metal ions (Ni^{2+} and Co^{2+}) from wastewater. The prepared composites were characterized by FTIR, SEM, and XRD to assess functional groups, morphologies, and structures. The nanocomposites were successfully synthesized as indicated by the presence of alumina silicate bonds in the nanocomposite spectrum and its XRD patterns. Adsorption of Ni^{2+} and Co^{2+} ions is best described by the Langmuir isotherm at higher pH values, as evidenced by a coefficient of correlation close to 1. The influence of pH and initial concentration of metal ions was confirmed through the removal yield results at different values of these parameters (pH = 3, 4.5, and 6; C_o = 20, 60, 100, 140, and 180). The following operating parameter values were selected as suitable for Co^{2+} uptake: pH 6 and an initial concentration of 60 ppm using the PAM/Na-MMT nanocomposite (4:1 w/w). For Ni^{2+} ions, the highest removal yield was reached at pH 6 and C_o of 100 ppm using the PAM/Na-MMT nanocomposite (2:1 w/w). These results were higher than those obtained by polyacrylamide and nanoclay under the same conditions (removal yield between 87.40 and 94.50%), suggesting that PAM/Na-MMT nanocomposites can be used more efficiently in heavy metal ion adsorption from aqueous solution.

APPENDIX

Appendix 1

Fitting results for isotherms during Ni^{2+} ions adsorption are shown in Figure A1.

Appendix 2

Fitting results for isotherms during Co^{2+} ions adsorption are shown in Figure A2.

AUTHOR INFORMATION

Corresponding Author

*E-mail: kmorenos@unicartagena.edu.co.

ORCID

Kariana Moreno-Sader: 0000-0002-7149-5333

João B. P. Soares: 0000-0001-8017-143X

Author Contributions

[§]K.M.-S. and A.G.-P. contributed equally to this work.

Notes

The authors declare no competing financial interest.

ACKNOWLEDGMENTS

Authors would like to thank the University of Cartagena and the University of Alberta for providing financial support to perform this research work.

REFERENCES

(1) Pal, S.; Ghorai, S.; Dash, M. K.; Ghosh, S.; Udayabhanu, G. Flocculation properties of polyacrylamide grafted carboxymethyl guar gum (CMG-g-PAM) synthesised by conventional and microwave assisted method. *J. Hazard. Mater.* **2011**, *192*, 1580−1588.

(2) Fu, F.; Wang, Q. Removal of heavy metal ions from wastewaters: A review. *J. Environ. Manage.* **2011**, *92*, 407−418.

(3) Bhattacharyya, K. G.; Gupta, S. S. Adsorption of a few heavy metals on natural and modified kaolinite and montmorillonite: A review. *Adv. Colloid Interface Sci.* **2008**, *140*, 114−131.

(4) Barakat, M. A. New trends in removing heavy metals from industrial wastewater. *Arabian J. Chem.* **2011**, *4*, 361−377.

(5) Vareda, J. P.; Valente, A. J. M.; Durães, L. Heavy metals in Iberian soils: Removal by current adsorbents/amendments and prospective for aerogels. *Adv. Colloid Interface Sci.* **2016**, *237*, 28−42.

(6) Kyzas, G. Z.; Deliyanni, E. A.; Matis, K. A. Activated carbons produced by pyrolysis of waste potato peels: Cobalt ions removal by adsorption. *Colloids Surf., A* **2016**, *490*, 74−83.

(7) Kang, R.; Qiu, L.; Fang, L.; et al. A novel magnetic and hydrophilic ion-imprinted polymer as a selective sorbent for the removal of cobalt ions from industrial wastewater. *Biochem. Pharmacol.* **2016**, *4*, 2268−2277.

(8) Tirtom, V. N.; Becerik, S.; Aydemir, T.; Çelik, A. Comparative adsorption of Ni (II) and Cd (II) ions on epichlorohydrin crosslinked chitosan − clay composite beads in aqueous solution. *Chem. Eng. J.* **2012**, *197*, 379−386.

(9) Machado, M. D.; Santos, M. S. F.; Gouveia, C.; Soares, H. M. V. M.; Soares, E. V. Removal of heavy metals using a brewer's yeast strain of *Saccharomyces cerevisiae*: The flocculation as a separation process. *Bioresour. Technol.* **2008**, *99*, 2107−2115.

(10) Atta, A. M.; Al-Lohedan, H. A.; ALOthman, Z. A.; Abdel-Khalek, A. A.; Tawfeek, A. M. Characterization of reactive amphiphilic montmorillonite nanogels and its application for removal of toxic cationic dye and heavy metals water pollutants. *J. Ind. Eng. Chem.* **2015**, *31*, 374−384.

(11) Hashem, A.; Ahmad, F.; Fahad, R. Application of some starch hydrogels for the removal of mercury(II) ions from aqueous solutions. *Adsorpt. Sci. Technol.* **2008**, *26*, 563−579.

(12) Kahraman, H. T. Development of an adsorbent via chitosan nano-organoclay assembly to remove hexavalent chromium from wastewater. *Int. J. Biol. Macromol.* **2017**, *94*, 202−209.

(13) Peng, W.; Li, H.; Liu, Y.; Song, S. A review on heavy metal ions adsorption from water by graphene oxide and its composites. *J. Mol. Liq.* **2017**, *230*, 496−504.

(14) Wong, S. S.; Teng, T. T.; Ahmad, A. L.; Zuhairi, A.; Najafpour, G. Treatment of pulp and paper mill wastewater by polyacrylamide (PAM) in polymer induced flocculation. *J. Hazard. Mater.* **2006**, *135*, 378−388.

(15) Nasser, M. S.; James, A. E. The effect of polyacrylamide charge density and molecular weight on the flocculation and sedimentation behaviour of kaolinite suspensions. *Sep. Purif. Technol.* **2006**, *52*, 241−252.

(16) Mishra, S.; Mukul, A.; Sen, G.; Jha, U. Microwave assisted synthesis of polyacrylamide grafted starch (St-g-PAM) and its applicability as flocculant for water treatment. *Int. J. Biol. Macromol.* **2011**, *48*, 106−111.

DOI: 10.1021/acsomega.9b00981
ACS Omega 2019, 4, 10834−10844

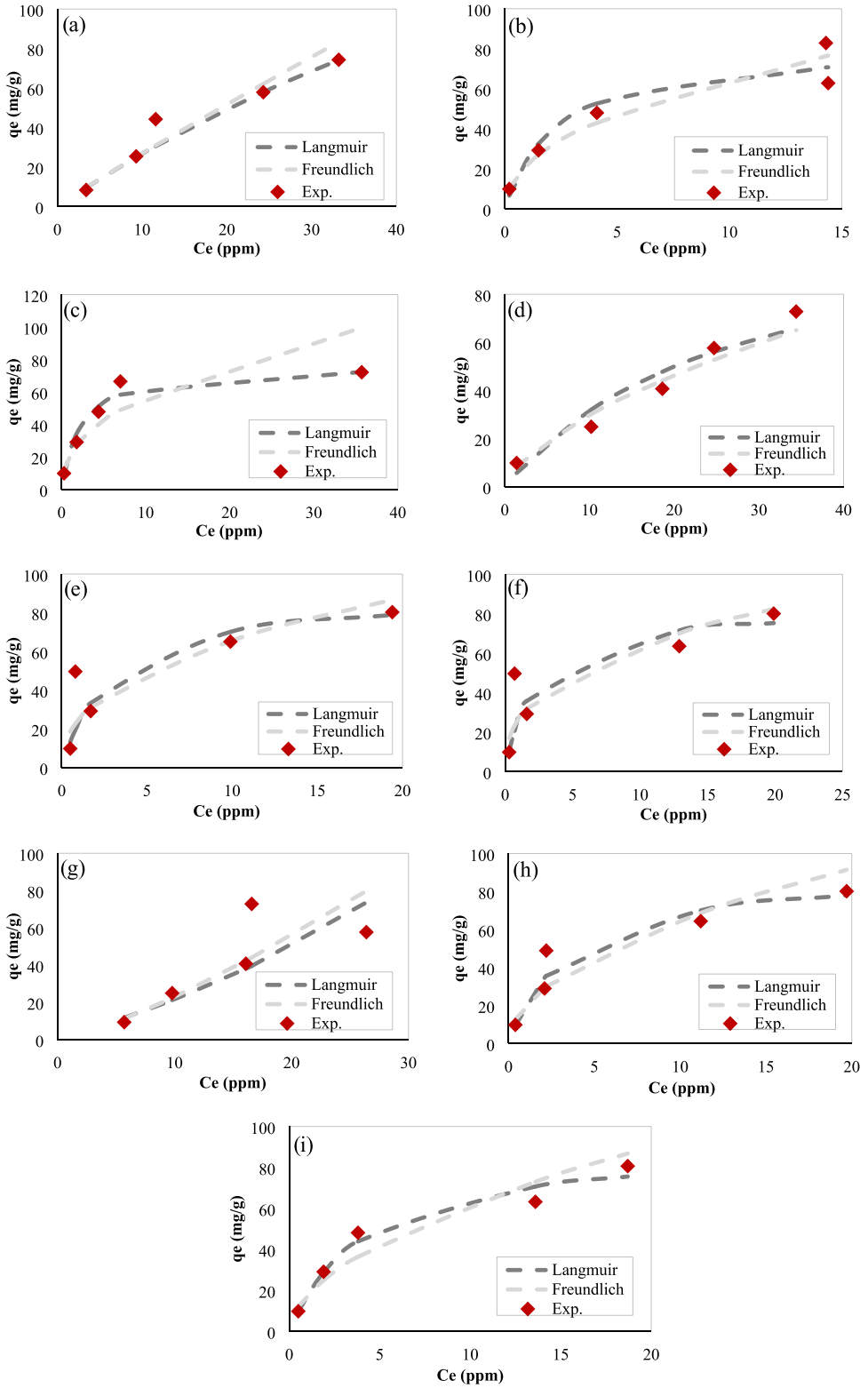

Figure A1. Fitting results for isotherms during Ni^{2+} ions adsorption: (a) PAM/Na-MMT nanocomposite (1:1) at pH 3, (b) PAM/Na-MMT nanocomposite (1:1) at pH 4.5, (c) PAM/Na-MMT nanocomposite (1:1) at pH 6, (d) PAM/Na-MMT nanocomposite (2:1) at pH 3, (e) PAM/Na-MMT nanocomposite (2:1) at pH 4.5, (f) PAM/Na-MMT nanocomposite (2:1) at pH 6, (g) PAM/Na-MMT nanocomposite (4:1) at pH 3, (h) PAM/Na-MMT nanocomposite (4:1) at pH 4.5, and (i) PAM/Na-MMT nanocomposite (4:1) at pH 6.

(17) Starodubtsev, S. G.; Lavrentyeva, E. K.; Shtykova, E. V.; Dembo, K. A.; Volkov, V. V. Montmorillonite − polycation multilayers incorporated in polyacrylamide. *Appl. Clay Sci.* **2009**, *46*, 88−94.

(18) Tseng, R. Physical and chemical properties and adsorption type of activated carbon prepared from plum kernels by NaOH activation. *J. Hazard. Mater.* **2007**, *147*, 1020−1027.

DOI: 10.1021/acsomega.9b00981
ACS Omega 2019, 4, 10834−10844

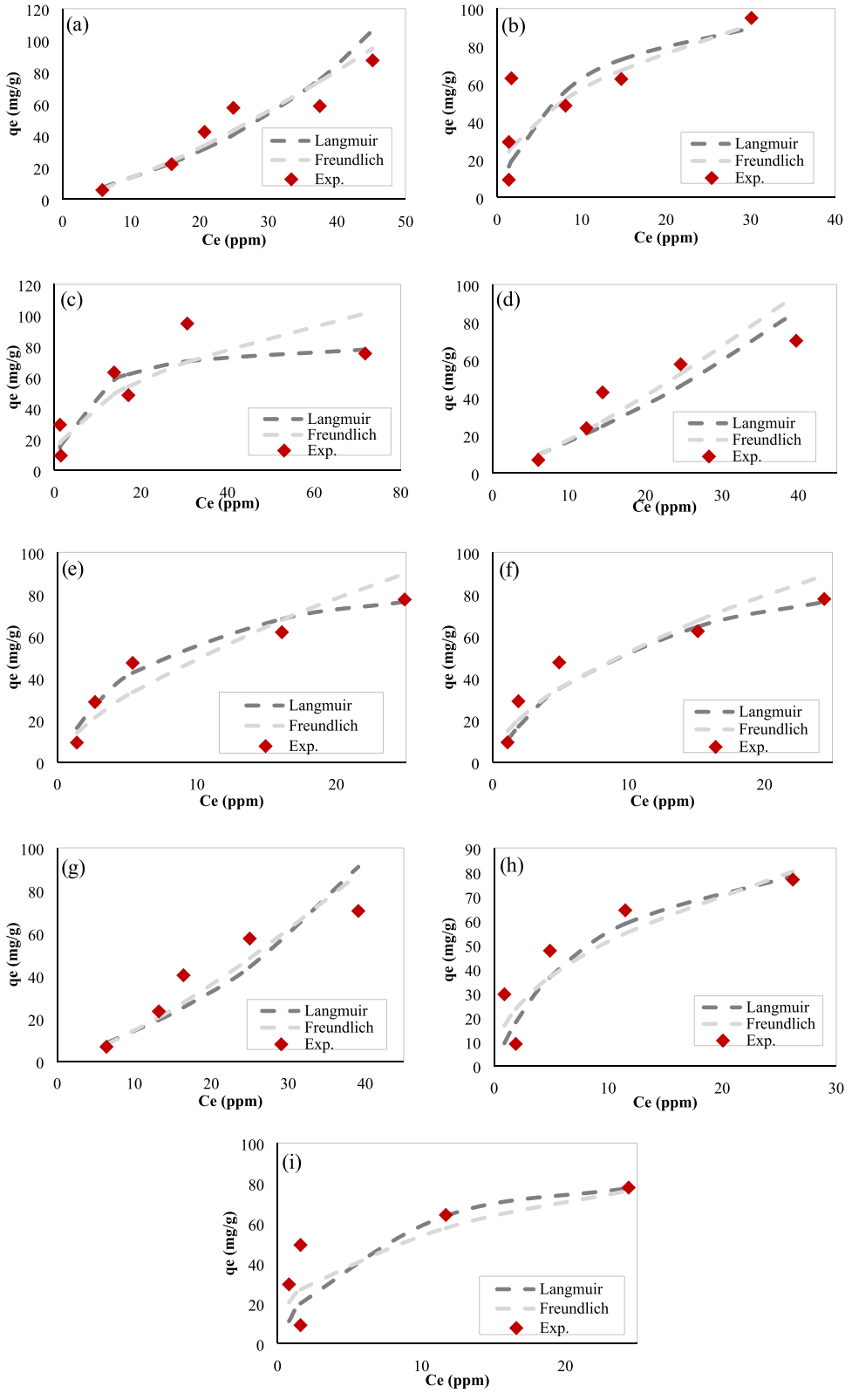

Figure A2. Fitting results for isotherms during Co^{2+} ions adsorption: (a) PAM/Na-MMT nanocomposite (1:1) at pH 3, (b) PAM/Na-MMT nanocomposite (1:1) at pH 4.5, (c) PAM/Na-MMT nanocomposite (1:1) at pH 6, (d) PAM/Na-MMT nanocomposite (2:1) at pH 3, (e) PAM/Na-MMT nanocomposite (2:1) at pH 4.5, (f) PAM/Na-MMT nanocomposite (2:1) at pH 6, (g) PAM/Na-MMT nanocomposite (4:1) at pH 3, (h) PAM/Na-MMT nanocomposite (4:1) at pH 4.5, and (i) PAM/Na-MMT nanocomposite (4:1) at pH 6.

(19) Hayati, B.; Maleki, A.; Naja, F.; Daraei, H.; Gharibi, F.; Mckay, G. Synthesis and characterization of PAMAM/CNT nanocomposite as a removal from wastewater. *J. Mol. Liq.* **2016**, *224*, 1032−1040.

(20) Zhao, G.; Zhang, H.; Fan, Q.; et al. Sorption of copper (II) onto super-adsorbent of bentonite − polyacrylamide composites. *J. Hazard. Mater.* **2010**, *173*, 661−668.

DOI: 10.1021/acsomega.9b00981
ACS Omega 2019, 4, 10834−10844

(21) Zaharia, A.; Sarbu, A.; Radu, A.; et al. Preparation and characterization of polyacrylamide-modi fi ed kaolinite containing poly [acrylic acid-co-methylene bisacrylamide] nanocomposite hydrogels. *Appl. Clay Sci.* **2015**, *103*, 46−54.
(22) Haraguchi, K. Nanocomposite hydrogels. *Curr. Opin. Solid State Mater. Sci.* **2007**, *11*, 47−54.
(23) Zohreh, A.; Gomez, V. G. Synthesis and characterization of polyacrylamide with controled molecular weight 2015.
(24) Jain, R.; Mahto, V. Evaluation of polyacrylamide/clay composite as a potential drilling fluid additive in inhibitive water based drilling fluid system. *J. Pet. Sci. Eng.* **2015**, *133*, 612−621.
(25) Caulfield, M.; Qiao, G.; Solomon, D. Some aspects of the properties and degradation of polyacrylamides. *Chem. Rev.* **2002**, *102*, 3067−3084.
(26) Matsuda, D. K. M.; Verceheze, A. E. S.; Carvalho, G. M.; Yamashita, F.; Mali, S. Baked foams of cassava starch and organically modified nanoclays. *Ind. Crops Prod.* **2013**, *44*, 705−711.
(27) Gao, Y.; Dai, Y.; Zhang, H.; Diao, E.; Hou, H.; Dong, H. Effects of organic modification of montmorillonite on the performance of starch-based nanocomposite films. *Appl. Clay Sci.* **2014**, *99*, 201−206.
(28) Silva, S.; Braga, C.; Fook, M.; Raposo, C.; Carvalho, L.; Canedo, E. Application of Infrared Spectroscopy to Analysis of Chitosan/Clay Nanocomposites. In *Infrared Spectroscopy - Materials Science, Engineering and Technology*; Theophanides, T., Ed.; InTech, 2012.
(29) Madejová, J.; Bujdák, J.; Janek, M.; Komadel, P. Comparative FT-IR study of structural modifications during acid treatment of dioctahedral smectites and hectorite. *Spectrochim. Acta, Part A* **1998**, *54*, 1397−1406.
(30) Deng, L.; Yuan, P.; Liu, D.; et al. Effects of microstructure of clay minerals, montmorillonite, kaolinite and halloysite, on their benzene adsorption behaviors. *Appl. Clay Sci.* **2017**, *143*, 184−191.
(31) Abdollahi, M.; Rezaei, M.; Farzi, G. A novel active bionanocomposite film incorporating rosemary essential oil and nanoclay into chitosan. *J. Food Eng.* **2012**, *111*, 343−350.
(32) Zaharia, A.; Sarbu, A.; Radu, A. L.; et al. Preparation and characterization of polyacrylamide-modified kaolinite containing poly [acrylic acid-co-methylene bisacrylamide] nanocomposite hydrogels. *Appl. Clay Sci.* **2015**, *103*, 46−54.
(33) Assaad, E.; Azzouz, A.; Nistor, D.; et al. Metal removal through synergic coagulation-flocculation using an optimized chitosan-montmorillonite system. *Appl. Clay Sci.* **2007**, *37*, 258−274.
(34) Vargas-Rodríguez, Y. M.; Gómez-Vidales, V.; Vázquez-Labastida, E.; et al. Caracterización espectroscópica, química y morfológica y propiedades superfi ciales de una montmorillonita mexicana. *Rev. Mex. Cienc. Geol.* **2008**, *25*, 135−144.
(35) Madejová, J.; Bujdák, J.; Janek, M.; Komadel, P. Comparative FT-IR study of structural modifications during acid treatment of dioctahedral smectites and hectorite. *Spectrochim. Acta, Part A* **1998**, *54*, 1397−1406.
(36) Bishop, J.; Murad, E.; Dyar, M. D. The influence of octahedral and tetrahedral cation substitution on the structure of smectites and serpentines as observed through infrared spectroscopy. *Clay Miner.* **2002**, *37*, 617−628.
(37) Li, X.; Kang, T.; Cho, W.; Lee, J.; Ha, C. Preparation and characterization of poly(butyleneterephthalate)/organoclay nanocomposites. *Macromolecules* **2001**, *22*, 1306−1312.
(38) Bilgiç, C.; Topaloğlu Yazici, D.; Karakehya, N.; Çetinkaya, H.; Singh, A.; Chehimi, M. M. Surface and interface physicochemical aspects of intercalated organo-bentonite. *Int. J. Adhes. Adhes.* **2014**, *50*, 204−210.
(39) Wokadala, O. C.; Ray, S. S.; Bandyopadhyay, J.; Wesley-Smith, J.; Emmambux, N. M. Morphology, thermal properties and crystallization kinetics of ternary blends of the polylactide and starch biopolymers and nanoclay: The role of nanoclay hydrophobicity. *Polymer* **2015**, *71*, 82−92.
(40) Ayana, B.; Supratim, S.; Khatua, B. B. Highly exfoliated eco-friendly thermoplastic starch (TPS)/poly (lactic acid)(PLA)/clay nanocomposites using unmodified nanoclay. *Carbohydr. Polym.* **2014**, *110*, 430−439.
(41) Lee, J. Y.; Lee, H. K. Characterization of organobentonite used for polymer nanocomposites. *Mater. Chem. Phys.* **2004**, *85*, 410−415.
(42) Sinha Ray, S.; Bousmina, M. Biodegradable polymers and their layered silicate nanocomposites: In greening the 21st century materials world. *Prog. Mater. Sci.* **2005**, *50*, 962−1079.
(43) Huang, X.; Netravali, A. N. Characterization of Nano-Clay Reinforced Phytagel-Modified Soy Protein Concentrate Resin. *Biomacromolecules* **2006**, *7*, 2783−2789.
(44) Iman, M.; Maji, T. K. Effect of crosslinker and nanoclay on starch and jute fabric based green nanocomposites. *Carbohydr. Polym.* **2012**, *89*, 290−297.
(45) Park, J. H.; Jana, S. C. Mechanism of exfoliation of nanoclay particles in epoxy-clay nanocomposites. *Macromolecules* **2003**, *36*, 2758−2768.
(46) Turri, S.; Alborghetti, L.; Levi, M. Formulation and properties of a model two-component nanocomposite coating from organophilic nanoclays. *J. Polym. Res.* **2008**, *15*, 365−372.
(47) Vaia, R. A.; Giannelis, E. P. Lattice Model of Polymer Melt Intercalation in Organically-Modified Layered Silicates. *Macromolecules* **1997**, *30*, 7990−7999.
(48) Pandey, J. K.; Singh, R. P. Green Nanocomposites from Renewable Resources: Effect of Plasticizer on the Structure and Material Properties of Clay-filled Starch. *Starch - Stärke* **2005**, *57*, 8−15.
(49) Ma, J.; Shi, J.; Ding, H.; Zhu, G.; Fu, K.; Fu, X. Synthesis of cationic polyacrylamide by low-pressure UV initiation for turbidity water flocculation. *Chem. Eng. J.* **2017**, *312*, 20−29.
(50) Ahmad, M.; Manzoor, K.; Venkatachalam, P.; Ikram, S. Kinetic and thermodynamic evaluation of adsorption of Cu (II) by thiosemicarbazide chitosan. *Int. J. Biol. Macromol.* **2016**, *92*, 910−919.
(51) Zhao, Y.; Liu, F.; Qin, X. Adsorption of diclofenac onto goethite: Adsorption kinetics and effects of pH. *Chemosphere* **2017**, *180*, 373−378.
(52) Liang, X.; Wei, G.; Xiong, J.; et al. Adsorption isotherm, mechanism, and geometry of Pb (II) on magnetites substituted with transition metals. *Chem. Geol.* **2017**, *470*, 132−140.
(53) Lingamdinne, L. P.; Yang, J.; Chang, Y.; Reddy, J. Low-cost magnetized *Lonicera japonica* flower biomass for the sorption removal of heavy metals. *Hydrometallurgy* **2016**, *165*, 81−89.
(54) Wang, S.; Liu, Q.; Tan, X.; Xu, C.; Gray, M. R. Adsorption of asphaltenes on kaolinite as an irreversible process. *Colloids Surf., A* **2016**, *504*, 280−286.
(55) Huang, Z.; Li, Y.; Chen, W.; et al. Modified bentonite adsorption of organic pollutants of dye wastewater. *Mater. Chem. Phys.* **2017**, *202*, 266−276.

DOI: 10.1021/acsomega.9b00981
ACS Omega 2019, 4, 10834−10844